ANISOTROPIC TRAVELTIME TOMOGRAPHY OF DIFFRACTION ARRIVALS BASED ON EIKONAL EQUATION

YOGESH ARORA and ILYA TSVANKIN

Department of Geophysics, Center for Wave Phenomena, Colorado School of Mines, Golden, CO 80401, U.S.A. yayogesh@gmail.com

ABSTRACT

Arora, Y. and Tsvankin, I., 2020. Anisotropic traveltime tomography of diffraction arrivals based on eikonal equation. *Journal of Seismic Exploration*, 29: 455-475.

Seismic diffractions provide wide angular illumination of the subsurface and, therefore, can supplement reflections in estimation of the parameters of anisotropic media. Migration velocity analysis of reflection data is usually performed by minimizing residual moveout in common-image gathers. This approach, however, cannot be directly applied to diffractions. Here, we propose to use the linearized eikonal equation to carry out traveltime tomography of diffraction arrivals in VTI (transversely isotropic with a vertical symmetry axis) media. The eikonal equation makes it possible to compute diffraction traveltimes along with their derivatives with respect to the medium parameters. To solve the linearized eikonal equation for VTI media, we employ an efficient and robust second-order finite-difference (FD) methodology based on the Fast Marching method. The accuracy of the developed technique is verified by computing the traveltime perturbations caused by Gaussian parameter anomalies embedded in a homogeneous VTI background. Another test of the modeling methodology involves perturbing the parameters of the structurally complex VTI Marmousi model. Then we perform traveltime tomography of transmission data generated for a VTI medium with Gaussian anomalies in the P-wave normal-moveout (V_{nmo}) and horizontal (V_{hor}) velocities. Finally, the tomographic algorithm is applied to diffraction traveltimes from scatterers embedded in the VTI Marmousi model. We use structure-oriented smoothing filters to condition the inversion gradients, which yields more geologically consistent velocity models. To evaluate the stability of the algorithm, this test is repeated using noise-contaminated traveltimes.

KEY WORDS: diffracted waves, anisotropy, transverse isotropy, traveltime tomography, velocity analysis, eikonal equation, finite-difference approximation.

INTRODUCTION

Traveltime tomography is a common tool for building isotropic and anisotropic velocity models from surface seismic data (e.g., Tromp et al., 2005). This method has also been applied to data acquired in vertical seismic profiling (VSP) and crosshole surveys (Bregman et al., 1989). Here, we develop a tomographic algorithm for inverting traveltimes of diffracted waves with the goal of refining velocity fields for VTI media.

Separation of diffractions from more intensive reflected waves typically requires knowledge of the velocity model (Klem-Musatov et al., 1994; Khaidukov et al., 2004; Moser and Howard, 2008; Landa et al., 2008). These separation techniques, originally developed for isotropic models, are extended to anisotropic media by Arora and Tsvankin (2016, 2018). Here, we assume that diffraction separation is performed using the velocity model obtained from reflection tomography or other established techniques. Then diffraction traveltimes to be used in tomographic inversion can be picked from shot gathers obtained by demigrating diffraction-based depth images.

The key steps of traveltime tomography are accurate modeling of traveltimes and computation of the traveltime derivatives with respect to the model parameters. In principle, traveltime modeling can be carried out by employing well-established ray-tracing methods (Červený, 2005). The traveltime derivatives (gradients) with respect to the pertinent parameters of anisotropic media can also be obtained from ray theory (Chapman and Pratt, 1992). However, a major drawback of these methods is a limited ray coverage in the presence of strong spatial velocity variations (e.g., near salt bodies). Ray tracing also involves the cumbersome task of recomputing traveltimes and their gradients (Fréchet derivatives) from the ray coordinates to regular (Cartesian) grids. Alternatively, traveltimes can be modeled by solving the eikonal equation using finite-difference (FD) approximations (Vidale, 1990; Van Trier and Symes, 1991; Qin and Schuster, 1993; Cao and Greenhalgh, 1994; Sethian and Popovici, 1999). The Fast Marching (FM) method proposed by Sethian (1996) and the Fast Sweeping (FS) method presented by Zhao (2005) are among the most robust and efficient FD techniques for eikonal-based traveltime computation. Fomel (2004) applies the FM method to model P-wave traveltimes for VTI media, whereas Waheed et al. (2015a,b) employ the FS method for traveltime modeling in 2D tilted TI models and 3D tilted orthorhombic media.

Traveltime tomography can be performed using adjoint-state techniques where the gradients of the objective function are obtained implicitly using, for example, the FS method (Huang and Bellefleur, 2012; Waheed et al., 2016). The gradients also can be found explicitly by solving a linearized eikonal equation in which the intermediate step of computing the

adjoint-state variables is eliminated. Then traveltime tomography can be performed using the Gauss−Newton approximation (Li et al., 2013; Treister and Haber, 2016). This approach is particularly appealing in multiparameter tomographic inversion for anisotropic media.

Here, we perform traveltime tomography of diffraction data for VTI media by solving the linearized eikonal equation with a second-order finite-difference approximation. After verifying the accuracy of this numerical solution, tomography is tested on data transmitted through a Gaussian anomaly embedded in a homogeneous VTI medium. Inversion of diffraction traveltimes is parameterized in terms of the P-wave normal-moveout (V_{nmo}) and horizontal (V_{hor}) velocities, while the vertical velocity V_{P0} is fixed at its actual value. Then the tomographic algorithm is applied to traveltimes from scatterers embedded in the VTI Marmousi model. To regularize the inversion, the gradients of the objective function are preconditioned with structure-oriented smoothing.

MODELING METHODOLOGY

Eikonal equation in anisotropic media

The eikonal equation can be used to model the first-arrival traveltimes of pure modes in arbitrarily anisotropic media. For 2D transversely isotropic models, the eikonal equation can be written as:

$$|\nabla T|^2 = \frac{1}{V^2(\theta)},$$

$$\text{or} \left(\frac{\partial T}{\partial x}\right)^2 + \left(\frac{\partial T}{\partial z}\right)^2 = \frac{1}{V^2(\theta)},$$

$$T(x_s, z_s) = 0, \tag{1}$$

where T is the traveltime, (x_s, z_s) is the source location, and $V(\theta)$ is the phase velocity of the mode of interest as a function of the phase angle θ with the symmetry axis. The linearized form of eq. (1) is obtained by differentiating it with respect to the medium parameters (e.g., the velocities V_{nmo} and V_{hor}):

$$\nabla T \cdot \nabla \tau = -\frac{\nu}{V^3(\theta)},$$

$$\text{or} \quad \frac{\partial T}{\partial x}\frac{\partial \tau}{\partial x} + \frac{\partial T}{\partial z}\frac{\partial \tau}{\partial z} = -\frac{\nu}{V^3(\theta)}, \tag{2}$$

where $\tau = \partial T/\partial\lambda$ and $v = \partial V/\partial\lambda$ are the gradients (derivatives) of the traveltime and phase velocity with respect to the parameter λ.

Fast Marching Method

To solve eq. (1) on regular grids, one can use finite-difference approximations which produce a smooth traveltime distribution even in the presence of strong velocity variations. Here, we follow the Fast Marching method in applying an upwind FD scheme starting from the source location. At each grid point (i, j), the traveltimes are computed sequentially similarly to Dijkstra's (1959) shortest-path algorithm with the following approximation for the gradient operator in eq. (1) (Rouy and Tourin, 1992; Sethian and Popovici, 1999):

$$|\nabla T|^2 \approx \max(D_{ij}^{-x}T, -D_{ij}^{+x}T, 0)^2 + \max(D_{ij}^{-z}T, -D_{ij}^{+z}T, 0)^2, \quad (3)$$

where the operators $D_{ij}^{\pm x}$ and $D_{ij}^{\pm z}$ are obtained using a second-order finite-difference approximation (Rickett and Fomel, 1999; Franklin and Harris, 2001):

$$D_{ij}^{\pm x}T = \frac{\mp 3T_{i,j} \pm 4T_{i\pm 1,j} \mp T_{i\mp 2,j}}{2\Delta x},$$

$$D_{ij}^{\pm z}T = \frac{\mp 3T_{i,j} \pm 4T_{i,j\pm 1} \mp T_{i,j\mp 2}}{2\Delta z}. \quad (4)$$

Likewise, the gradient operators in eq. (2) are approximated as follows:

$$\nabla T \cdot \nabla\tau \approx \max(D_{ij}^{-x}T, -D_{ij}^{+x}T, 0)\max(D_{ij}^{-x}\tau, -D_{ij}^{+x}\tau, 0)$$
$$+ \max(D_{ij}^{-z}T, -D_{ij}^{+z}T, 0)\max(D_{ij}^{-z}\tau, -D_{ij}^{+z}\tau, 0). \quad (5)$$

Fomel (2004) implements eqs. (3) and (4) for VTI media in Madagascar (Fomel et al., 2013) program *sfeikonalvti*. To solve the linearized eikonal equation, we compute the traveltimes (T) for the background model using that code. The slownesses $D_{ij}^{\pm x}T$ and $D_{ij}^{\pm z}T$ in eq.(5) determine the phase direction for the wavefront propagation. Then this equation is solved for τ following the same sequence as the one employed to calculate the background traveltimes.

Computing traveltime perturbations

Eq. (2) can be used to obtain the traveltime perturbations δT as a function of the perturbations δV in the phase velocity. We use the following first-order approximation for the phase-velocity perturbation:

$$\delta V \approx \frac{\partial V}{\partial \lambda} \, \delta \lambda,$$

$$(6)$$

where λ is a medium parameter and $\delta \lambda$ is its perturbation. If necessary, eq. (6) can be replaced with a higher-order approximation in a straightforward way. The P-wave phase velocity is calculated from an approximate expression given by Alkhalifah (1998):

$$2V^2(\theta) \approx V_{\text{hor}}^2 \sin^2 \theta + V_{\text{P0}}^2 \cos^2 \theta + \sqrt{(V_{\text{hor}}^2 \sin^2 \theta + V_{\text{P0}}^2 \cos^2 \theta)^2 + V_{\text{P0}}^2 (V_{\text{nmo}}^2 - V_{\text{P0}}^2) \sin^2 2\theta},$$

$$(7)$$

where V_{P0}, $V_{\text{nmo}} = V_{\text{P0}}\sqrt{(1+2\delta)}$ and $V_{\text{hor}} = V_{\text{P0}}\sqrt{(1+2\varepsilon)}$ are the P-wave vertical, normal-moveout and horizontal velocities, respectively (ε and δ are Thomsen's anisotropy coefficients). These three parameters control the P-wave kinematics for vertical transverse isotropy. Alternatively, the acoustic VTI medium can be parameterized by the velocities V_{P0} and V_{hor} and the anellipticity parameter η responsible for P-wave time processing (Tsvankin, 2012),

$$\eta = \frac{\epsilon - \delta}{1 + 2\delta} \, .$$

$$(8)$$

Because the method introduced above is based on a first-order linearization, the perturbations in the medium parameters should be small enough for the phase direction to remain close to that for the background model.

To verify the accuracy of the proposed technique, we first use a background VTI model with the parameters of Greenhorn shale (Fomel, 2004) and introduce a Gaussian anomaly in V_{P0}, V_{hor}, or η. The corresponding traveltime perturbations (δT) are computed from eq. (2) using the background traveltimes (T_b) obtained from eq. (1) for a source located at $x = z = 0$ km (Fig. 1). For comparison, we also calculate the traveltimes (T) for the perturbed model directly with the FM method and subtract the background values to find the exact traveltime differences ($T - T_b$). We conduct three separate experiments by perturbing one VTI parameter at a

time, while the other two parameters are kept unchanged. The traveltime perturbations produced by the proposed linearized method are almost identical to the actual values (Figs. 2 - 4), and the sum $T_b + \delta T$ practically coincides with the traveltimes computed for the perturbed model. These tests demonstrate that our algorithm can accurately handle perturbations in all pertinent parameters with no numerical instability issues.
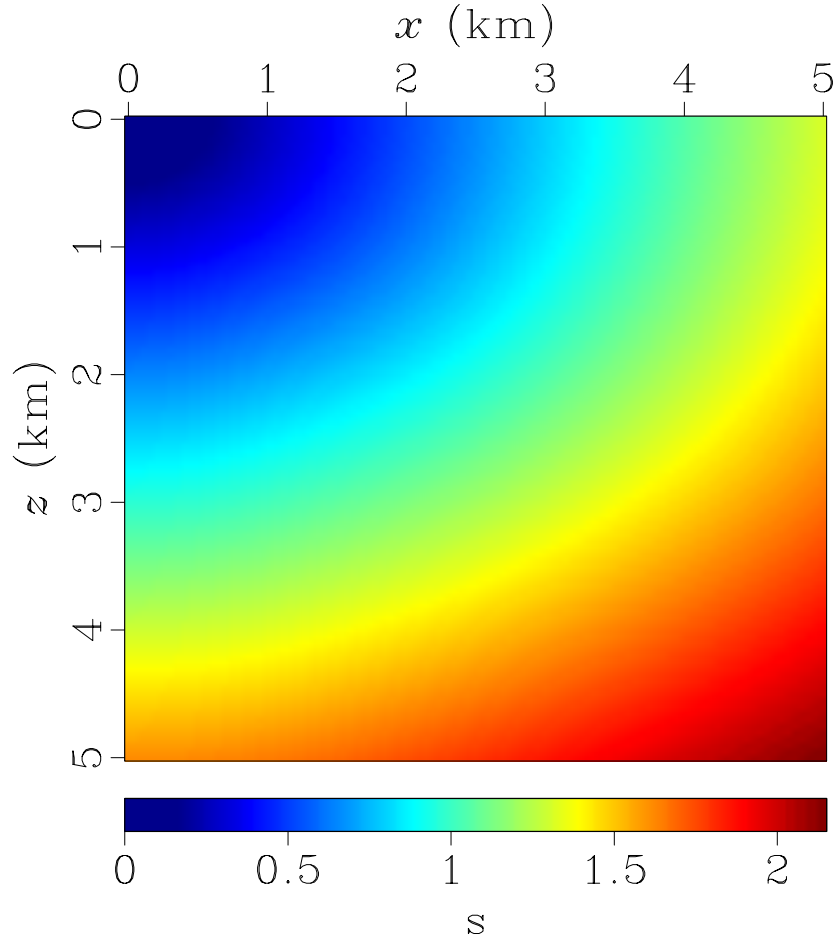

Fig. 1. Traveltimes (T_b) computed for a source located at $x = z = 0$ km in a homogeneous background VTI medium with $V_{P0} = 3.1$ km/s, $V_{hor} = 3.80$ km/s, and $\eta = 0.34$ (based on the model of Greenhorn shale).

Next, we use the structurally complex VTI Marmousi model as the background medium (Figs. 5 and 6). After perturbing one of the parameters, the corresponding traveltime perturbations are computed for a surface source located at $x = 3.68$ km using the algorithm described above (Figs. 7 - 9). As in the previous test, the traveltime perturbations are close to the actual traveltime differences computed with the FM method. Clearly, the proposed numerical scheme for solving the linearized eikonal equation is sufficiently accurate even in the presence of pronounced parameter perturbations caused by substantial heterogeneity.
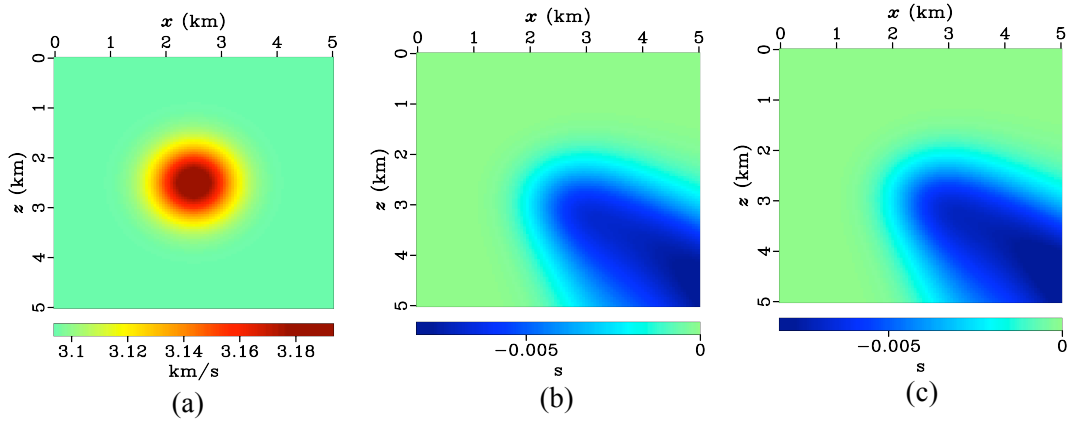
Fig. 2. (a) Perturbation in the vertical velocity V_{P0} for the model in Fig. 1. (b) The traveltime perturbations for the source at $x = z = 0$ km obtained from the linearized eikonal equation. (c) The traveltime differences between the perturbed and background models computed for the same source with the FM method.
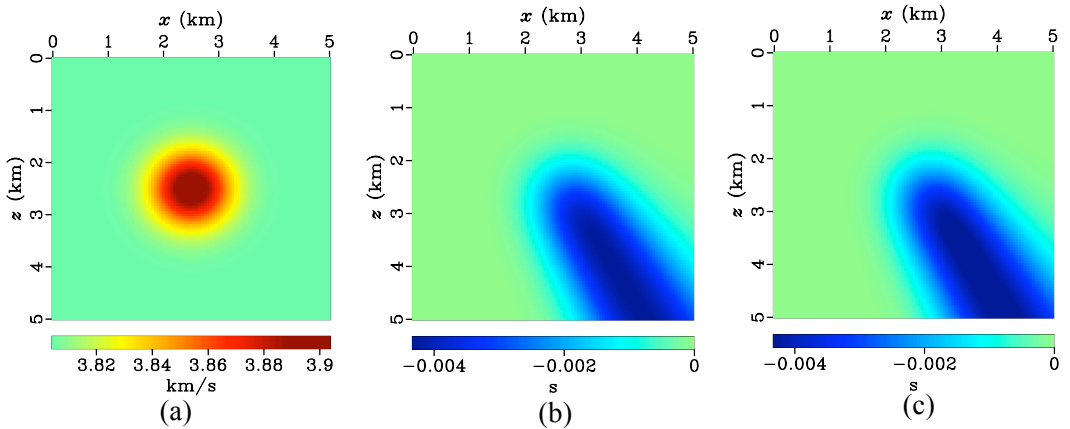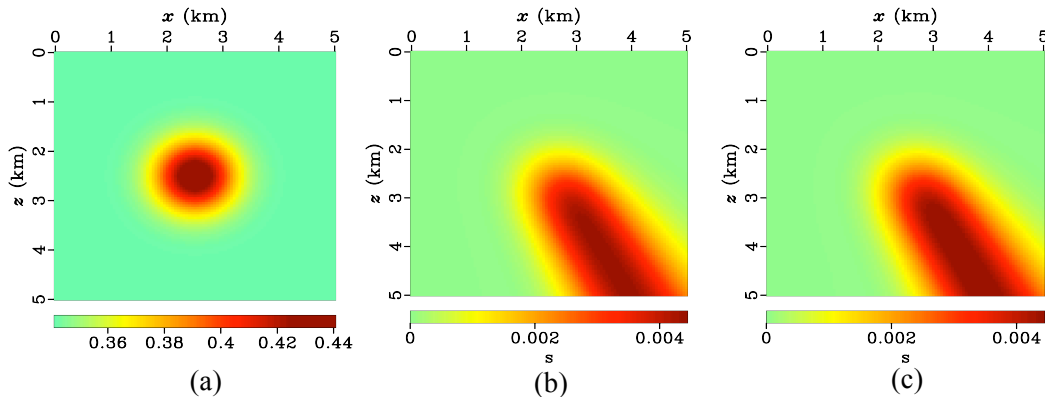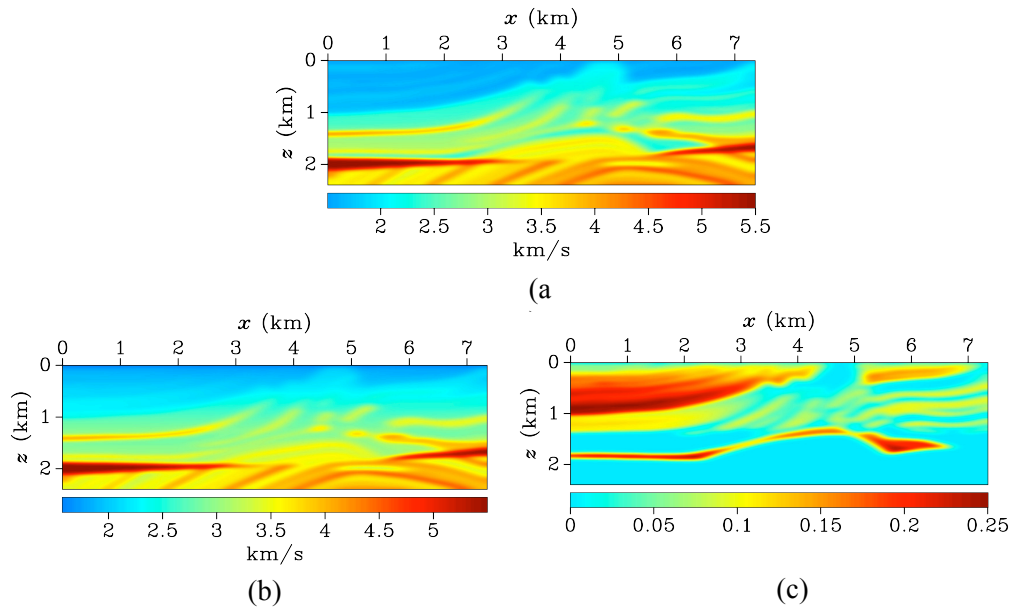

Fig. 3. (a) Perturbation in the horizontal velocity V_{hor} for the model in Fig. 1. (b) Traveltime perturbations for the source at $x = z = 0$ obtained from the linearized eikonal equation. (c) The traveltime differences between the perturbed and background models computed for the same source with the FM method.

Fig. 4. (a) Perturbation in the parameter η for the model in Fig. 1. (b) Traveltime perturbations for the source at $x = z = 0$ obtained from the linearized eikonal equation. (c) The traveltime differences between the perturbed and background models computed for the same source with the FM method.

Fig. 5. Smoothed parameters of the VTI Marmousi model: (a) V_{P0}, (b) V_{hor}, and (c) η.
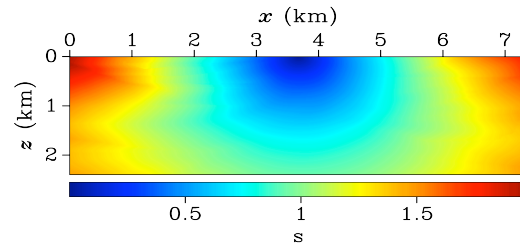

Fig. 6. Traveltimes computed with the FM method for a surface source located at $x =$ 3.68 km in the model from Fig. 5.
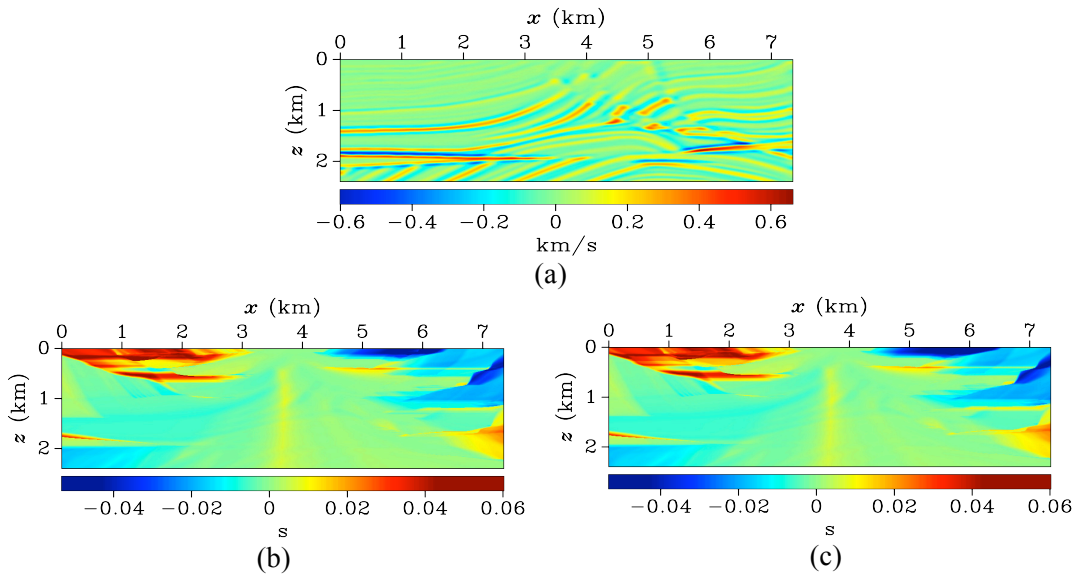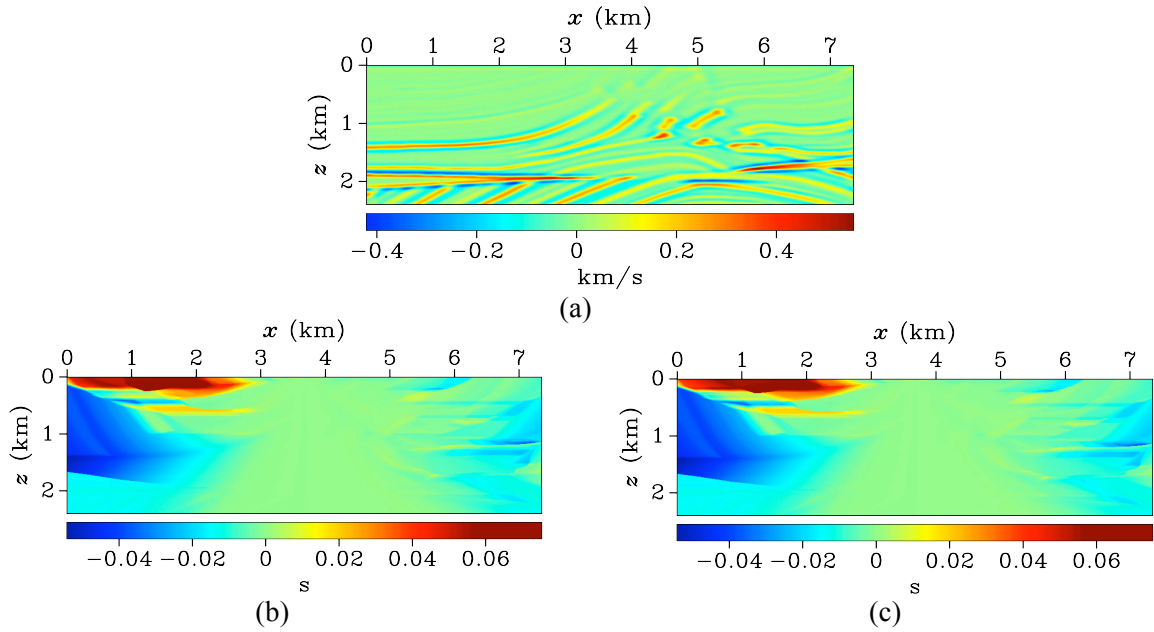

Fig. 7. (a) Perturbation in the velocity V_{P0} for the background model in Fig. 5. (b) The traveltime perturbations obtained from the linearized eikonal equation for a source located at ($x = 3.68$ km, $z = 0$ km). (c) The traveltime difference between the perturbed and background models computed for the same source with the FM method.
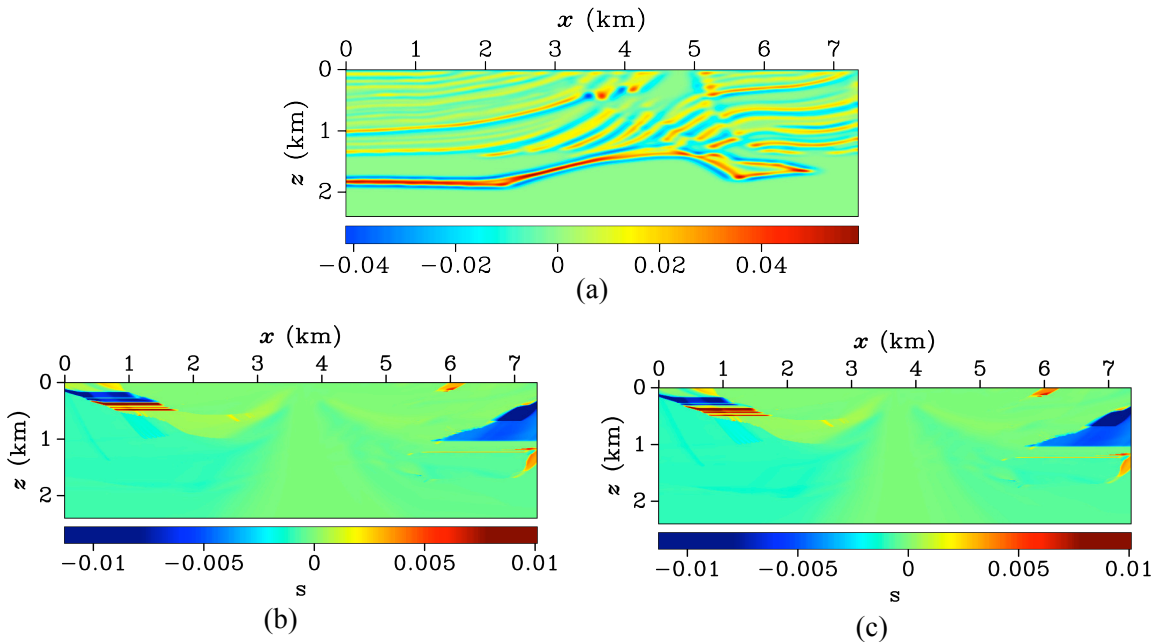
Fig. 8. (a) Perturbation in the velocity V_{hor} for the background model in Fig. 5. (b) The traveltime perturbations obtained from the linearized eikonal equation for a source located at ($x = 3.68$ km, $z = 0$ km). (c) The traveltime difference between the perturbed and background models computed for the same source with the FM method.

Fig. 9. (a) Perturbation in the anellipticity parameter η for the background model in Fig. 5. (b) The traveltime perturbations obtained from the linearized eikonal equation for a source located at ($x = 3.68$ km, $z = 0$ km). (c) The traveltime difference between the perturbed and background models computed for the same source with the FM method.

TRAVELTIME TOMOGRAPHY FOR DIFFRACTION ARRIVALS

The objective function in traveltime tomography is generally chosen as the l_2−norm of the difference between the observed (T^{obs}) and calculated (T^{cal}) traveltimes:

$$\mathcal{J}(\mathbf{m}) = \frac{1}{2}\|\mathbf{P}\, T^{\mathrm{cal}}(\mathbf{m}) - T^{\mathrm{obs}}\|_2, \tag{9}$$

where $\mathbf{m}$ is the vector of the medium parameters defined on a rectangular grid and $\mathbf{P}$ is an operator that projects the simulated traveltimes onto the receiver locations. By evaluating the derivatives of the objective function with respect to the model parameters, we find the inversion gradients as:

$$\nabla_{\mathbf{m}}\mathcal{J}(\mathbf{m}) = \mathbf{P}^T \left[\mathbf{P}\, T^{\mathrm{cal}}(\mathbf{m}) - T^{\mathrm{obs}}\right] \frac{\partial T^{\mathrm{cal}}(\mathbf{m})}{\partial \mathbf{m}}, \tag{10}$$

where $\mathbf{P}^T$ is the transpose of $\mathbf{P}$. The traveltime gradients with respect to the elements of the model vector ($\partial T^{\mathrm{cal}}(\mathbf{m})/\partial \mathbf{m}$), also known as the Fréchet derivatives, are used to construct the Jacobian matrix $\mathbf{J}$ for each source. We use the nonlinear conjugate gradient method to obtain the descent direction ($\Delta \mathbf{m}$) from the preconditioned gradient of the objective function:

$$\Delta \mathbf{m} = -\boldsymbol{\mathcal{P}}^{-1}\nabla_{\mathbf{m}}\mathcal{J}(\mathbf{m}), \tag{11}$$

where the preconditioner $\boldsymbol{\mathcal{P}}$ is computed from the diagonal elements of the matrix $\mathbf{J}^T\mathbf{J}$, which represents the Gauss-Newton approximation of the Hessian matrix. The algorithm inverts for the velocities V_{nmo} and V_{hor}, while the vertical velocity V_{P0} is fixed at its actual value because it can seldom be constrained by reflection or diffraction traveltimes in VTI media (Tsvankin, 2012). This parameterization is convenient for inversion because operating only with velocities makes it possible to have the same units of all model parameters and also of the gradients of the objective function. Model updating is performed as follows:

$$\mathbf{m}^+ = \mathbf{m}^- + \alpha \Delta \mathbf{m}, \tag{12}$$

where $\mathbf{m}^+$ and $\mathbf{m}^-$ denote the velocity models at the current and previous iterations, respectively, and α is an optimal step length obtained by employing the Wolfe conditions in the line search (Nocedal and Wright, 2006). Eqs. (11) and (12) are solved using an optimization toolbox provided by Métivier and Brossier (2016).

Test for Gaussian anomaly

For the first test, a Gaussian anomaly in the parameters V_{nmo} and V_{hor} is embedded in a homogeneous VTI background (Fig. 10). In this transmission experiment, the sources are placed at the surface and the receivers at the bottom of the model. The inversion for V_{nmo} and V_{hor} is performed using the methodology described above with the homogeneous background as the initial model. The Gaussian anomalies in the middle of the model are well-recovered (Fig. 11) but there are some spurious updates around them, which is a typical artifact of multiparameter anisotropic inversion. The data residuals and the objective function are significantly reduced by model updating (Figs. 12 and 13).

(a)

(b)
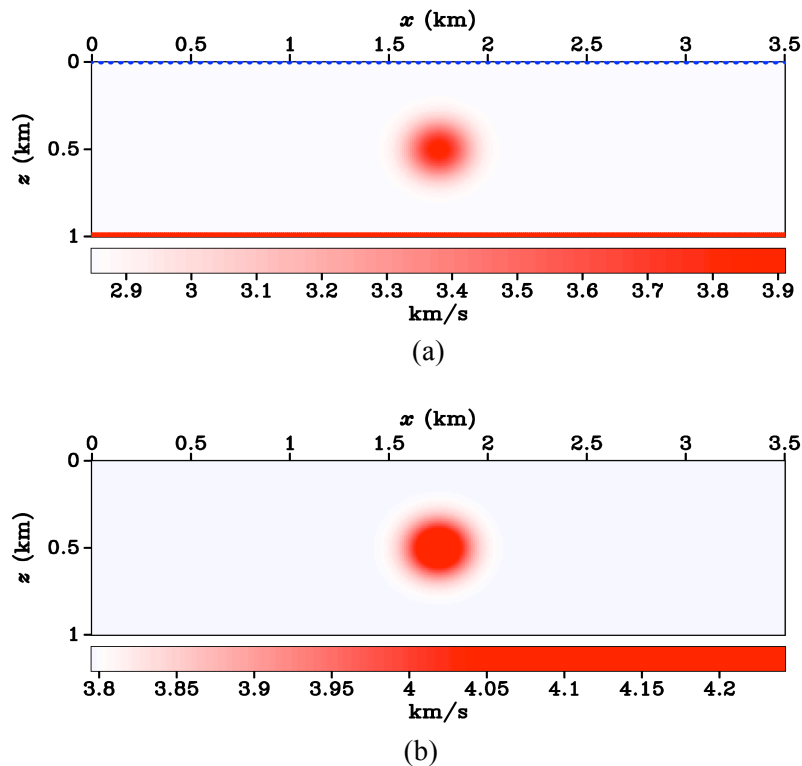
Fig. 10. Gaussian anomalies in the velocities (a) V_{nmo} and (b) V_{hor} embedded in a homogeneous VTI background with V_{P0} = 3.0 km/s, V_{nmo} = 2.86 km/s, and V_{hor} = 3.79 km/s.

Test for the VTI Marmousi model

The next test is carried out for the VTI Marmousi model (Alkhalifah, 1997; Fig. 14) with the sources placed at the scatterer locations obtained from diffraction-based depth images (Arora and Tsvankin, 2016, 2018). These scatterers are fixed at their actual locations during the inversion; however, these locations could be updated at each iteration using diffraction-

based seismic images produced by techniques discussed in Arora and Tsvankin (2016, 2018). The traveltime tomography of the diffraction arrivals recorded at the surface is performed starting from a 1D initial model (Fig. 15). Although the inversion adequately recovers low-wavenumber features of the model (Fig. 16), there are some structural distortions between $x = 0$ and $x = 2$ km, likely caused by poor illumination and/or limited acquisition aperture. The tomographic model updating substantially reduces the data residuals (Fig. 17) and the objective function (Fig. 18) in about 10 iterations.

(a)

(b)
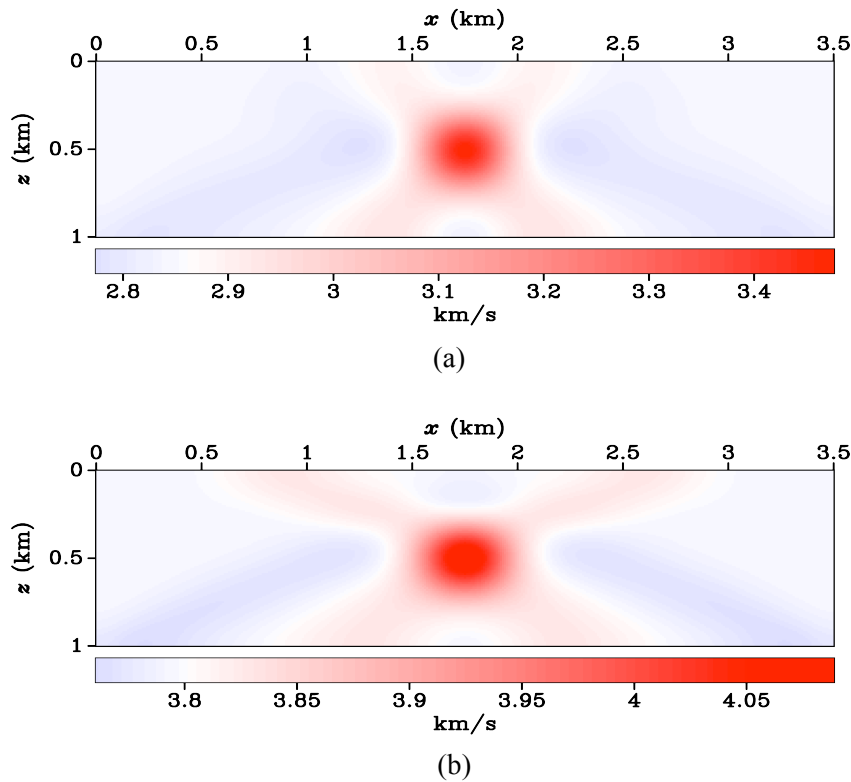
Fig. 11. Inverted parameters (a) V_{nmo} and (b) V_{hor} for the model in Fig. 10. The background VTI medium is used as the initial model.

To mitigate geologically inconsistent model updates, next we smooth the inversion gradients using structure-oriented filters (Hale, 2009). The structural information is obtained from migrated images computed with the velocity model estimated at the latest iteration of the inversion (Wang and Tsvankin, 2013; Li et al., 2019). The smoothing substantially improves the spatial distribution of the inverted parameters (Fig. 19), whereas the data residuals and the objective function are reduced similarly to those in the previous experiment (Figs. 20 and 21). Also, the focusing of reflectors in the migrated image generated using the inverted model is noticeably improved compared to that for the initial model (Fig. 22).
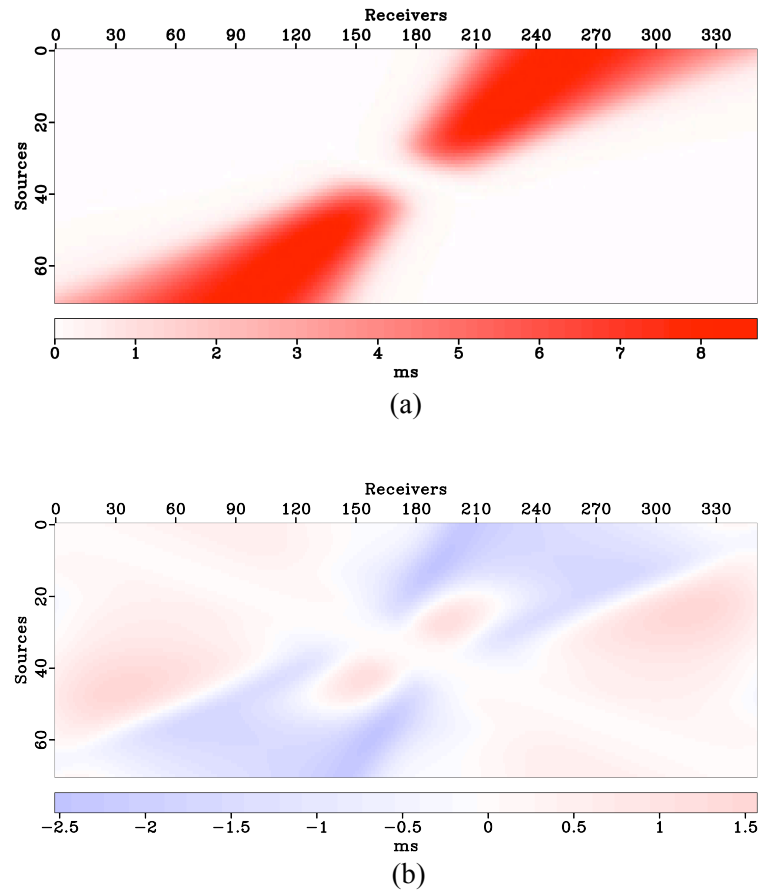
(a)

(b)

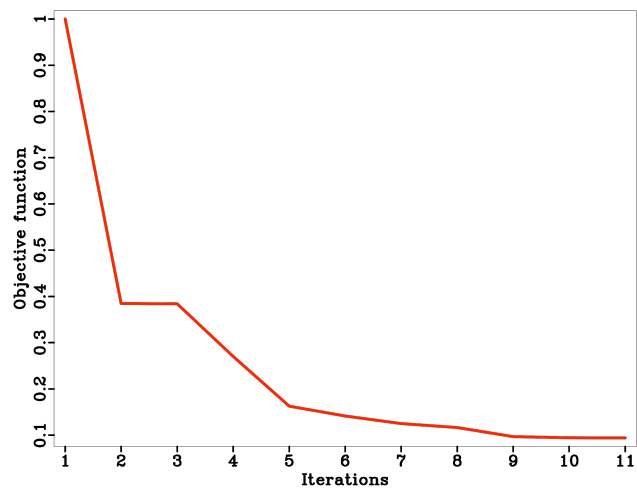Fig. 12. Data residuals in the source-receiver coordinates (a) before and (b) after the inversion.

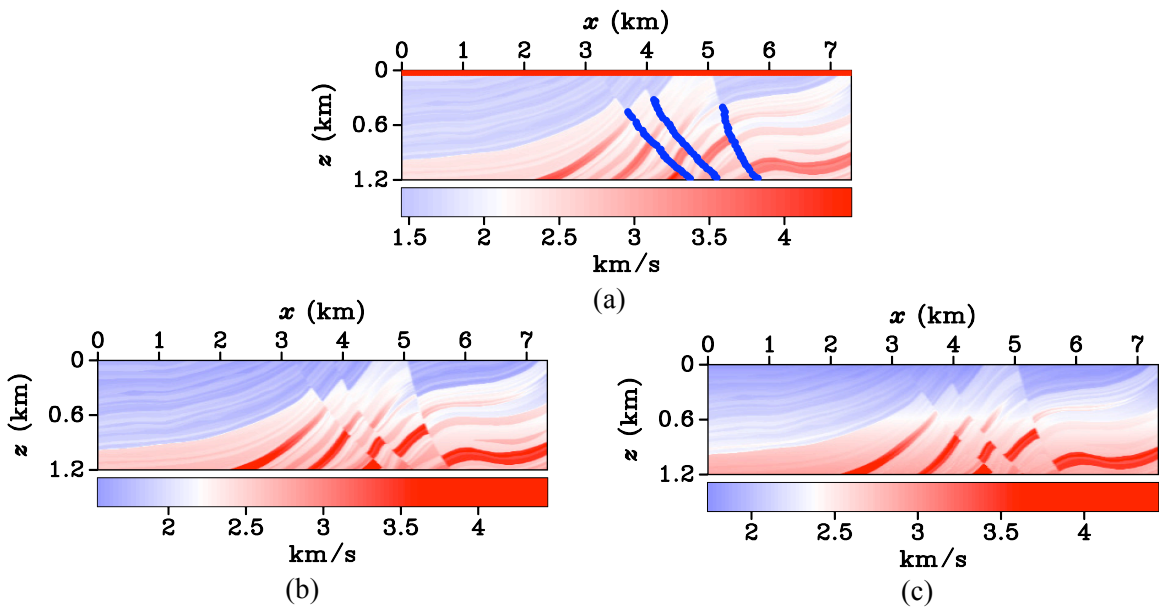Fig. 13. Reduction of the objective function with the iterations for the model in Fig. 10.

Fig. 14. Parameters (a) V_{P0}, (b) V_{nmo}, and (c) V_{hor} of the VTI Marmousi model. Diffraction traveltimes are computed for the scatterers marked in blue, and recorded by the receivers in red.
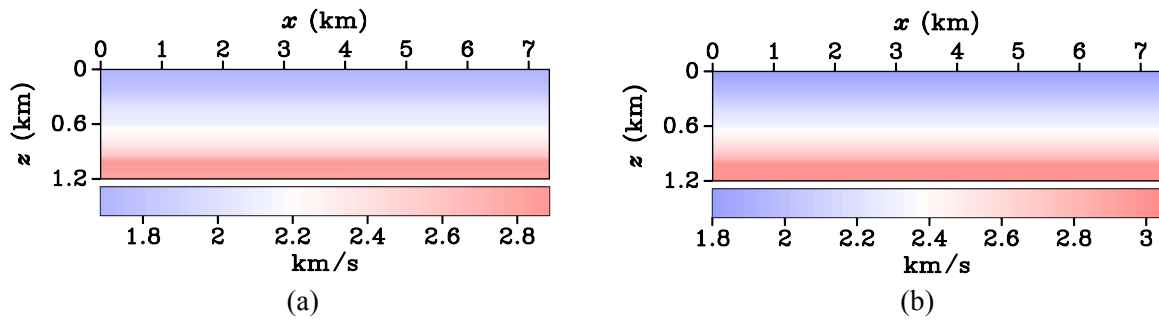

Fig. 15. Initial parameters (a) V_{nmo} and (b) V_{hor} for the Marmousi model. The vertical velocity V_{P0} is fixed at its actual value.
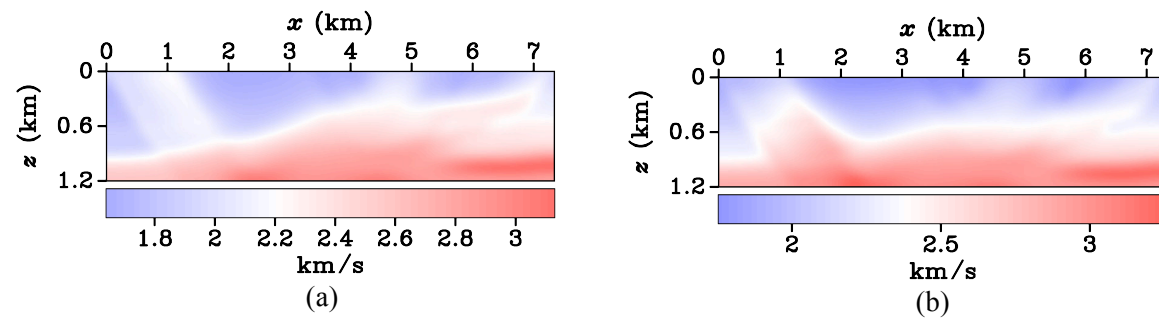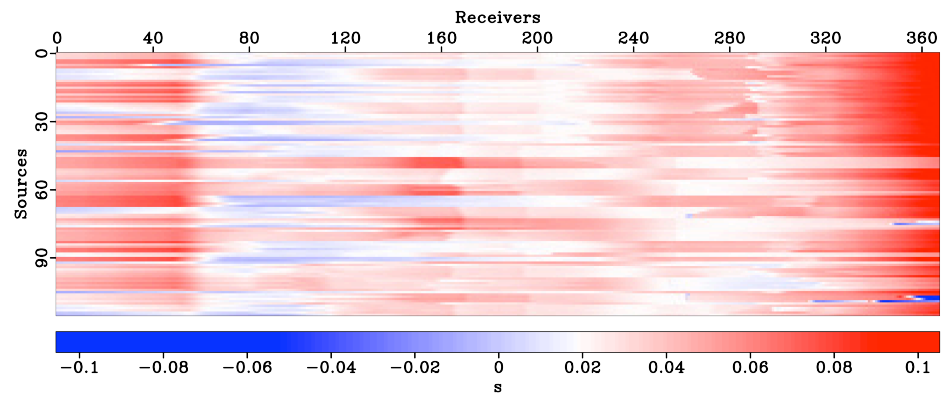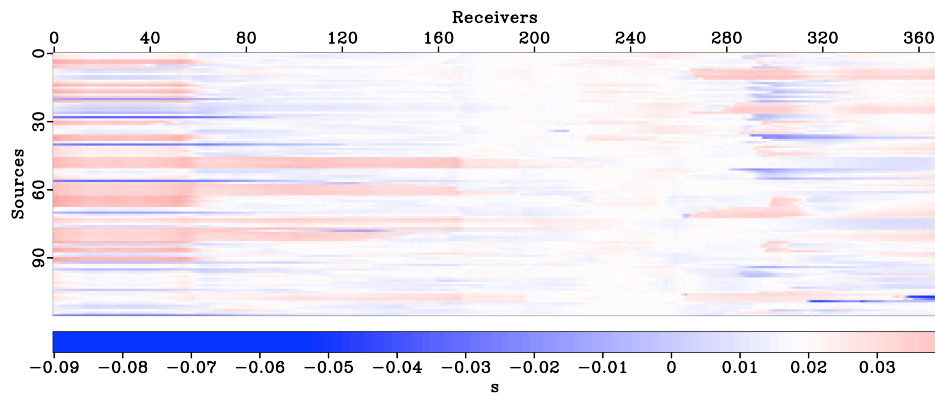

Fig. 16. Inverted parameters (a) V_{nmo} and (b) V_{hor}.

(a)

(b)

Fig. 17. Data residuals in the source-receiver coordinates (a) before and (b) after the inversion for the model in Fig. 14.
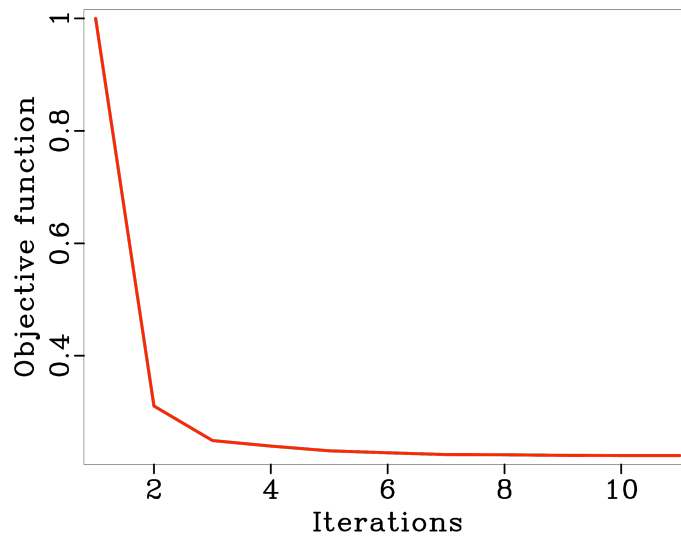

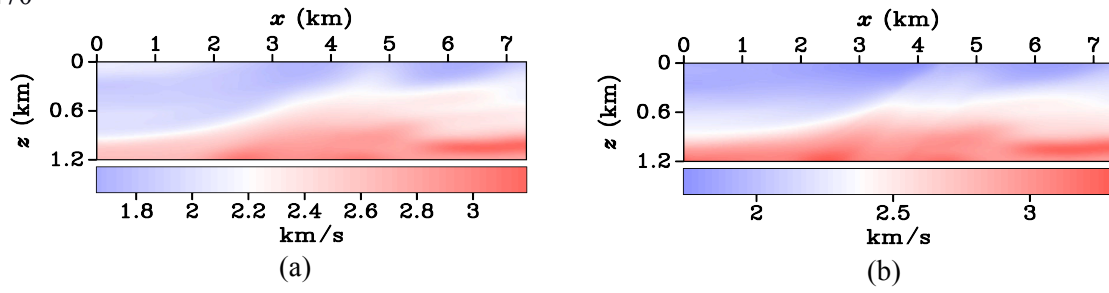Fig. 18. Reduction of the objective function for the model in Fig. 14.

Fig. 19. Inverted parameters (a) V_{nmo} and (b) V_{hor} obtained after application of structure-oriented smoothing.
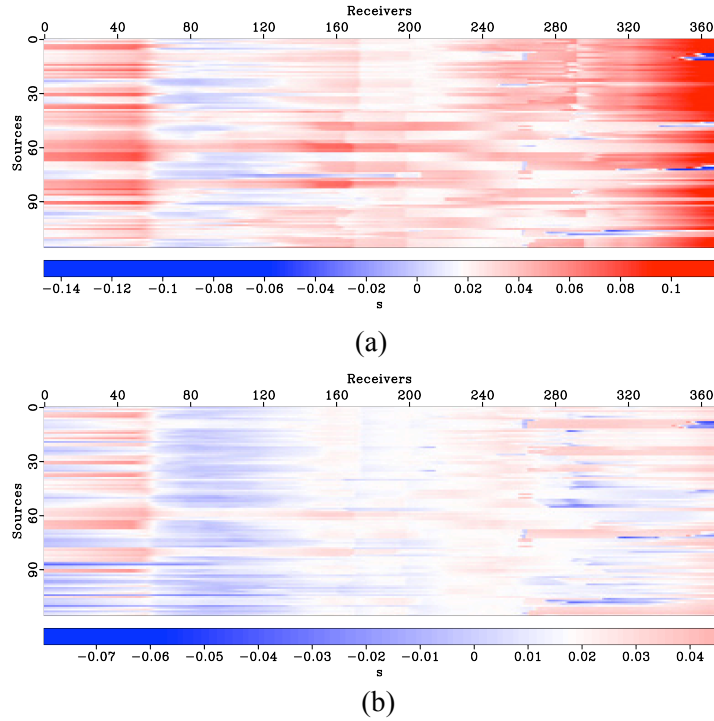

Fig. 20. Data residuals in the source-receiver coordinates (a) before and (b) after the inversion with structure-oriented smoothing for the model in Fig. 14.
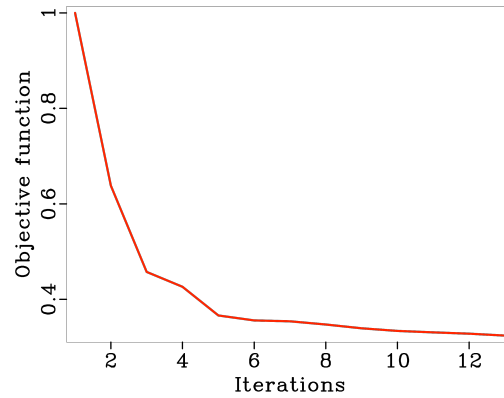

Fig. 21. Reduction of the objective function with iterations for the model in Fig. 14 after application of structure-oriented smoothing.
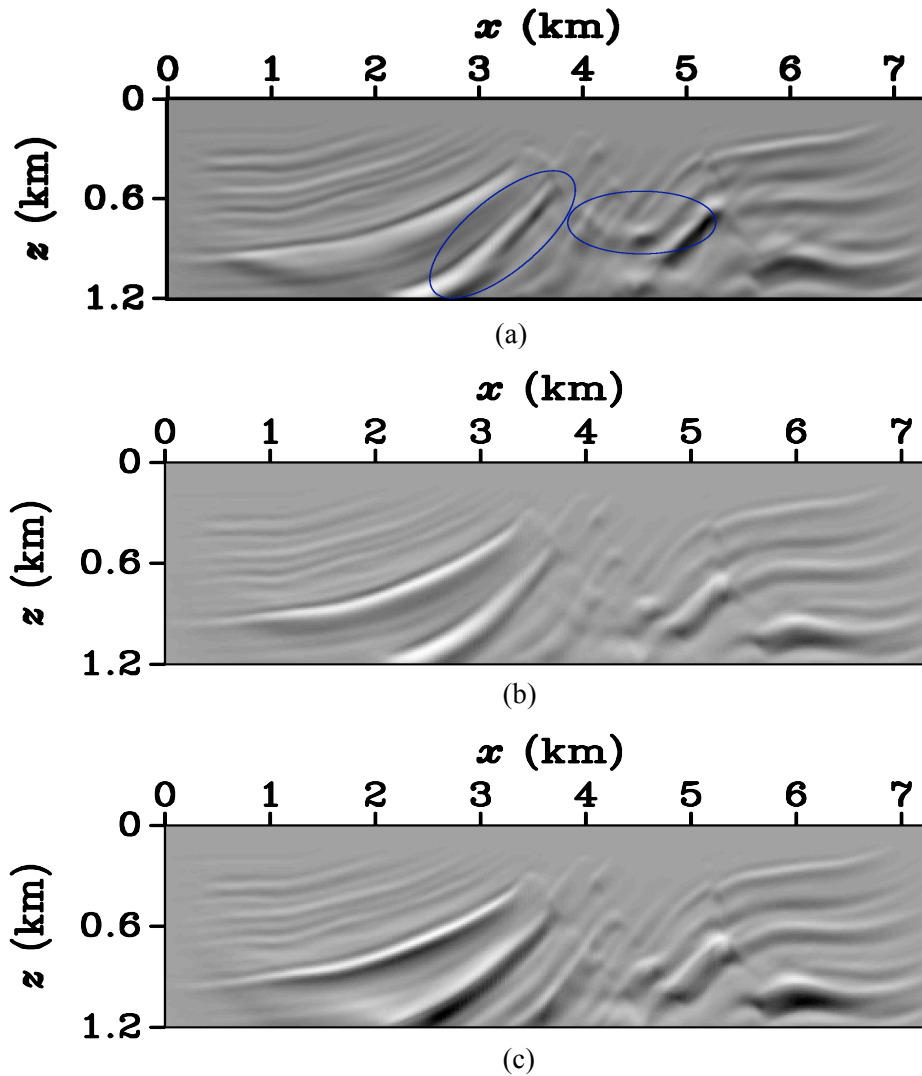
Fig. 22. Images obtained by Kirchhoff prestack depth migration using (a) the initial model in Fig. 15; (b) the inverted model in Fig. 19, and (c) the actual model in Fig. 14.

This test is repeated by adding to the observed traveltimes Gaussian noise with the signal-to-noise ratio of approximately 20 dB (the maximum errors of ±40 ms in traveltimes with 11 ms standard deviation). In practice, such noise could be caused by errors in separating diffractions and in picking diffraction traveltimes, as well as by inaccurate locations of the scatterers due to insufficiently focused depth images. The low-wavenumber components of the V_{nmo}-field are mostly recovered but there are some noise-related inconsistent updates in the velocity V_{hor} in the shallow part of the section between $x = 3$ and 4 km (Fig. 23). As expected, the traveltime residuals for the noisy data are not reduced as much as in the previous experiment (Fig. 24), and the convergence of the objective function becomes slower due to errors in the inversion gradients (Fig. 25). Still, this test confirms the applicability of the proposed methodology to field data of sufficiently high quality.

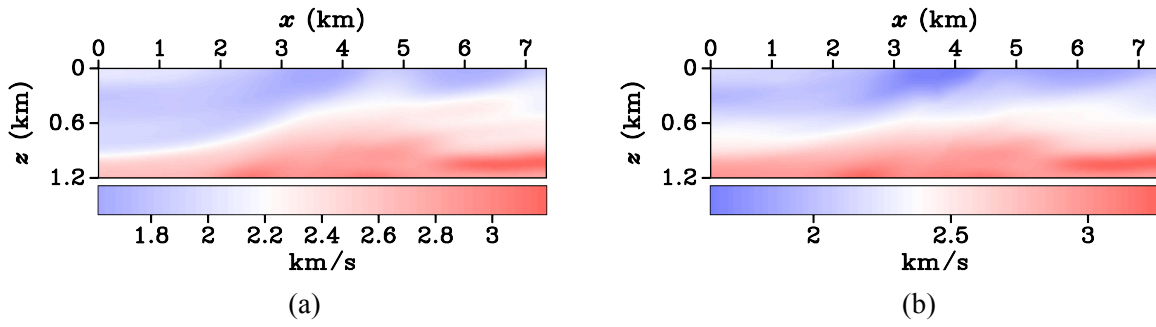Fig. 23. Inverted parameters (a) V_{nmo} and (b) V_{hor} obtained from noisy traveltimes.
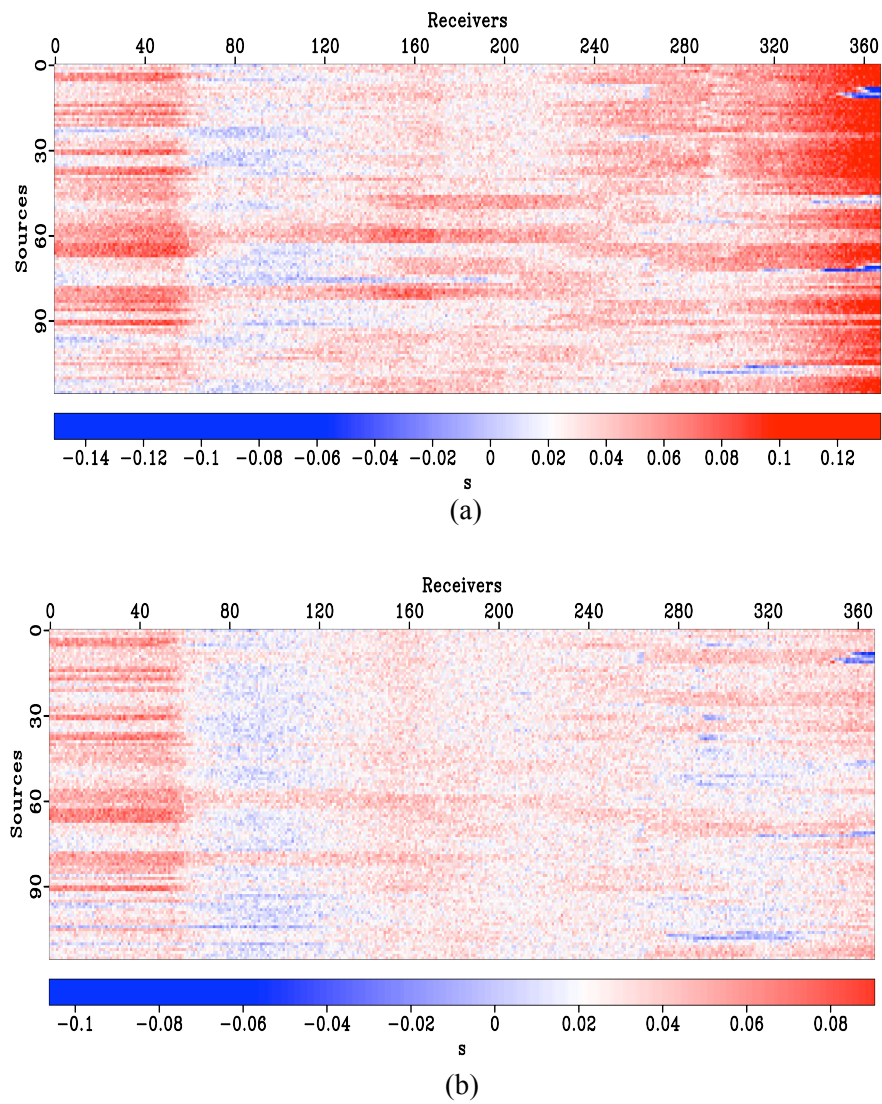

Fig. 24. Data residuals in the source-receiver coordinates (a) before and (b) after the inversion of noisy traveltimes for the model in Fig. 14.
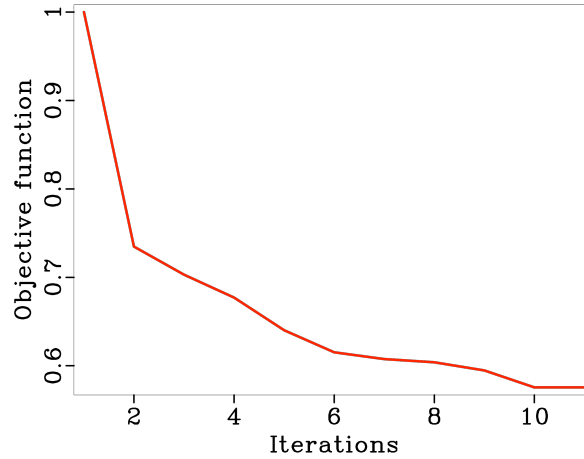
Fig. 25. Reduction of the objective function with iterations in the presence of noise for the model in Fig. 14.

CONCLUSIONS

We developed traveltime tomography of diffraction arrivals for VTI media based on the linearized eikonal equation. This equation is solved with second-order finite-differences in a way similar to the Fast Marching (FM) method. The accuracy of the obtained solution is verified by modeling the traveltime perturbations caused by Gaussian anomalies in the parameters V_{P0}, V_{hor}, and η responsible for P-wave kinematics in VTI media. The traveltimes for both the background and perturbed models were also obtained by solving the exact eikonal equation with the FM method. The results of both computations are almost identical, which confirms the robustness of the proposed modeling algorithm for typical values of the anisotropy coefficients. This test was successfully repeated for the structurally complex VTI Marmousi model.

The feasibility of using the linearized eikonal equation for traveltime tomography was evaluated by reconstructing the Gaussian anomalies in the NMO (V_{nmo}) and horizontal (V_{hor}) velocities from transmission traveltimes. Then the velocities V_{nmo} and V_{hor} were estimated from the traveltimes of diffraction arrivals produced by scatterers embedded in the VTI Marmousi model. The velocity V_{P0} was fixed at its actual value but it could be estimated as well if borehole information is available. Conditioning of the model updates by structure-oriented smoothing of the gradients of the objective function produced geologically consistent velocity models. These inversion results, as well as those for noise-contaminated input traveltimes, confirm that diffractions can help to refine anisotropic velocity models, if diffraction traveltimes can be reliably estimated from surface seismic data. The scatterers' locations, which were assumed to be known, could be potentially updated along with the velocity model.

REFERENCES

Alkhalifah, T., 1997. An anisotropic Marmousi model: SEP-95. Stanford Exploration Project: 265- 282.

Alkhalifah, T., 1998. Acoustic approximations for processing in transversely isotropic media. Geophysics, 63, 623-631.

Arora, Y. and Tsvankin, I., 2016. Separation of diffracted waves in transversely isotropic media. Studia Geophys. Geodaet., 60: 487-499.

Arora, Y. and Tsvankin, I., 2018. Analysis of diffractions in dip-angle gathers for transversely isotropic media. J. Seismic Explor., 27: 515-530.

Bregman, N., Bailey, R. and Chapman, C., 1989. Crosshole seismic tomography. Geophysics, 54: 200-215.

Cao, S. and Greenhalgh, S., 1994. Finite-difference solution of the eikonal equation using an efficient, first-arrival, wavefront tracking scheme. Geophysics, 59: 632-643.

Červený, V., 2005. Seismic Ray Theory. Cambridge University Press, Cambridge.

Chapman, C. and Pratt, R., 1992. Traveltime tomography in anisotropic media - I. Theory. Geophys. J. Internat., 109: 1-19.

Dijkstra, E.W., 1959. A note on two problems in connexion with graphs. Numer. Mathemat., 1: 269-271.

Fomel, S., 2004. On anelliptic approximations for qP velocities in VTI media. Geophys. Prosp., 52: 247-259.

Fomel, S., Sava, P., Vlad, I., Liu, Y. and Bashkardin, V., 2013. Madagascar: Open-source software project for multidimensional data analysis and reproducible computational experiments. J. Open Res. Softw., 1.

Franklin, J.B. and Harris, J.M., 2001. A high-order fast marching scheme for the linearized eikonal equation. J. Computat. Acoust., 9: 1095-1109.

Hale, D., 2009. Structure-oriented smoothing and semblance. CWP report, 635: 261-270.

Huang, J.-W. and Bellefleur, G., 2012. Joint transmission and reflection traveltime tomography using the fast sweeping method and the adjoint-state technique. Geophys. J. Internat., 188: 570-582.

Khaidukov, V., Landa, E. and Moser, T.J., 2004. Diffraction imaging by focusing-defocusing: An outlook on seismic superresolution. Geophysics, 69: 1478-1490.

Klem-Musatov, K.D., Hron, F., Lines, L.R. and Meeder, C.A., 1994. Theory of Seismic Diffractions. SEG, Tulsa, OK.

Landa, E., Fomel, S. and Reshef, M., 2008. Separation, imaging, and velocity analysis of seismic diffractions using migrated dip-angle gathers. Expanded Abstr., 78th Ann. Internat. SEG Mtg., Las Vegas.

Li, S., Vladimirsky, A. and Fomel, S., 2013. First-break traveltime tomography with the double-square-root eikonal equation. Geophysics, 78(6): U89-U101.

Li, V., Guitton, A.,Tsvankin, I. and Alkhalifah, T., 2019. Image-domain wavefield tomography for VTI media. Geophysics, 84(2): C119-C128.

Métivier, L. and Brossier, R., 2016. The seiscope optimization toolbox: A large-scale nonlinear optimization library based on reverse communication. Geophysics, 81(2): F1-F15.

Moser, T. and Howard, C., 2008. Diffraction imaging in depth. Geophys. Prosp., 56: 627- 641.

Nocedal, J. and Wright, S., 2006. Numerical Optimization, 2nd ed. Springer Science & Business Media, New York.

Qin, F. and Schuster, G.T., 1993. First-arrival traveltime calculation for anisotropic media. Geophysics, 58: 1349-1358.

Rickett, J. and Fomel, S., 1999. A second-order fast marching eikonal solver. Stanford Exploration Project Report, 100: 287-293.

Rouy, E. and Tourin, A., 1992. A viscosity solutions approach to shape-from-shading. SIAM J. Numer. Analys., 29: 867-884.

Sethian, J.A., 1996. A fast marching level set method for monotonically advancing fronts. Proc. Nation. Acad. Sci., 93: 1591-1595.

Sethian, J.A. and Popovici, A.M., 1999, Three-dimensional traveltimes computation using the fast marching method. Geophysics, 64: 516-523.

Treister, E. and Haber, E., 2016. A fast marching algorithm for the factored eikonal equation. J. Computat. Phys., 324: 210-225.

Tromp, J., Tape, C. and Liu, Q., 2005. Seismic tomography, adjoint methods, time reversal and banana-doughnut kernels. Geophys. J. Internat., 160: 195-216.

Tsvankin, I., 2012. Seismic Signatures and Analysis of Reflection Data in Anisotropic Media, 3rd Ed. SEG, Tulsa, OK.

Van Trier, J. and Symes, W.W., 1991. Upwind finite-difference calculation of traveltimes. Geophysics, 56: 812-821.

Vidale, J.E., 1990. Finite-difference calculation of traveltimes in three dimensions. Geophysics, 55: 521-526.

Waheed, U.B., Alkhalifah, T. and Wang, H., 2015a. Efficient traveltime solutions of the acoustic TI eikonal equation. J. Computat. Phys., 282: 62-76.

Waheed, U.B., Yarman, C.E. and Flagg, G., 2015b. An iterative, fast-sweeping-based eikonal solver for 3D tilted anisotropic media. Geophysics, 80(3): C49-C58.

Waheed, U.B., Flagg, G. and Yarman, C.E., 2016. First-arrival traveltime tomography for anisotropic media using the adjoint-state method. Geophysics, 81(4): R147-R155.

Wang, X. and Tsvankin, I., 2013. Multiparameter TTI tomography of P-wave reflection and VSP data. Geophysics, 78(5): WC51-WC63.

Zhao, H., 2005. A fast sweeping method for eikonal equations. Mathemat. Computat., 74: 603-627.